

Nanosecond Pulse Electroporator With Silicon Carbide MOSFETs: Development and Evaluation

Eva Pirc , Damijan Miklavčič , and Matej Reberšek 

Abstract—Nanosecond electroporation of cell organelles is being studied since more than a decade, but it is still not entirely understood. Unique prototype hardware equipment and challenging measuring methods may also be a contributing reason for this situation. In the scope of this paper, we improve the performance of the high-voltage nanosecond pulse generator by introducing silicon carbide (SiC) MOSFETs. We developed a new high-voltage diode opening switch (DOS)—nanosecond pulse generator for laboratory use for *in vitro* experiments in electroporation cuvettes. Analysis and comparison of the most commonly used switching technologies in pulse generators were made. The device is designed by two parallel two-stage Marx-bank circuits with SiC MOSFETs that generates up to 200 A in the resonant network. A driving circuit for stable simultaneous switching of SiC MOSFETs was developed. The developed generator can deliver from 500 V to more than 6 kV, approximately 8 ns pulses to a 50 Ω load. Even though the amplitude of the output pulse is not as high as expected, the multiplication factor V_{OUT}/V_{IN} is still approximately 9, which is an improvement compared to the previously published linear DOS generator. Measurement and evaluation process is described in detail. Additionally, we emphasize on the size of an error that occurs during measurements.

Index Terms—Electroporator, nanosecond pulse generator, silicon carbide power MOSFET, diode opening switch (DOS), nanosecond pulse measurement.

I. INTRODUCTION

ELECTROPORATION is a technique in which electric pulses are applied to tissue or cells, in order to increase permeability of their membranes [1]–[3]. In case of reversible electroporation the membrane becomes permeable to molecules, that otherwise cannot pass the barrier and can subsequently fully recover, opposed to the main goal of irreversible electroporation that is cell death. Electroporation is already established

in medicine and biotechnology [4], [5], electrochemotherapy (ECT) is used to introduce chemotherapeutic drug into cells [6]–[8] and IRE (irreversible electroporation) to induce cell death, thus to ablate tissue [9], [10]. Overall electroporation is a technique with great potential [5], [11]–[16]. Applied electric pulses induce voltage across the cell membrane that is pulse duration and amplitude dependent. The same amount of electroporated cells can be reached, with shorter pulse duration, if higher pulse amplitude is used [17]. The shorter the pulses are, the easier they “penetrate” into cell interior and permeabilize internal membranes of organelles [18]. The application requires electroporator to generate and electrodes to deliver electrical pulses to tissue or cells. An electroporator is a high-voltage pulse generator that generates pulses of specific shape, amplitude, duration, number and pulse repetition rate [19], [20]. It is very important to adjust pulse parameters to specific tissues, cell types, applications and desired outcomes. Most of the devices available on the market generate pulses with lengths from 10 μ s to 10 ms, at an electric field strength in the range of several hundreds of volts per centimeter. Pulses from 100 to 900 μ s duration, with similar electric field strengths are widely used for electrochemotherapy. Nanosecond pulses (4–600) ns long, with electric field strengths of several tens of kilo-volts per centimeter, are able to affect membranes of internal organelles [21]–[23].

There are five major concepts of electroporator design, capacitor discharge, square wave pulse generator, analog generators, pulse forming network, and diode opening switches [19], [20]. First three concepts are mostly, used to generate micro- and milli-second pulses. For nanosecond pulse generation pulse forming networks or transmission lines and DOS (Diode Opening Switch) are more appropriate solutions. All pulse power devices as well as electroporators work in two phases: charge and discharge. During charging period switches are turned off and transmission lines or capacitors are charged. When the switches are turned on, capacitors discharge to the output load [19].

In electroporation device design, we are looking for switching elements that generate maximum load current in this short on stage and are at the same time capable of fast synchronous reproducible, switching at high-voltages and currents. Semiconductor switching elements that were most often used in nanosecond pulse electroporators are radio-frequency (RF) MOSFETs in pulse-forming network concepts and power MOSFETs or IGBTs in DOS concepts. RF MOSFETs enable fast switching while

Manuscript received July 10, 2018; revised November 20, 2018 and January 12, 2019; accepted March 15, 2019. Date of publication March 25, 2019; date of current version November 20, 2019. This work was supported by the Slovenian Research Agency (ARRS) (MRIC UL IP-0510, P2-0249, funding for Junior Researchers to E. Pirc, bilateral project BI-FR/16-17-PROTEUS), and conducted within the scope of the European Associated Laboratory on the Electroporation in Biology and Medicine (LEA-EBAM). (Corresponding author: Matej Reberšek.)

E. Pirc and D. Miklavčič are with the Faculty of Electrical Engineering, University of Ljubljana.

M. Reberšek is with the Faculty of Electrical Engineering, University of Ljubljana, Ljubljana SI-1000, Slovenia (e-mail: matej.rebersek@fe.uni-lj.si).

Digital Object Identifier 10.1109/TBME.2019.2907165

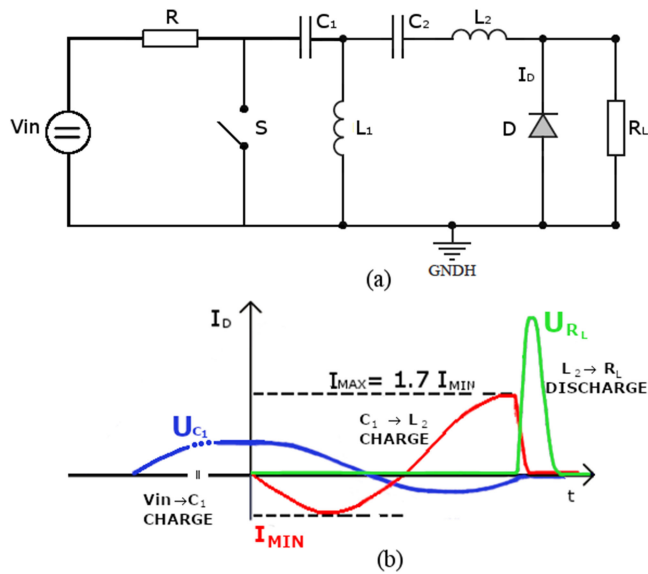


Fig. 1. Basic schematics of Diode Opening Switch – DOS and its operation. Diode D with a good repeatability transfers energy saved in the second inductor L_2 to the load R_L (a). Diode must be forward and reverse pumped, with adequate anharmonic current I_D and should stop conducting when all energy is stores in L_2 , at this time a maximal reverse current through the diode I_{MAX} is equal to $1.7 * I_{MIN}$. If all the conditions are met, a short high-voltage pulse U_{RL} is induced on the load (b).

power MOSFETs and IGBTs are slower, but enable high currents. Between semiconductor materials that are used for construction of switching elements that work from 1200 V to 6500 V, which is area of our interest, wide energy band-gap materials such as silicon carbide (SiC) are more and more commonly used [24], [25]. Elements that are based on wide energy band-gap materials, have much lower leakage currents, higher operating temperatures and better radiation hardness. Therefore higher critical electric fields can be reached, consequently blocking layers can be thinner and with higher doping concentration. Therefore, SiC MOSFETs also have lower on-resistance and electrons in saturation can reach higher velocities, which results in higher operating frequencies. Additionally good thermal conductivity enables operation at higher power densities [24], [26]. However, modest transconductance and short channel effects are important to be considered, when using the device. Due to their excellent properties, SiC MOSFETs are replacing silicon IGBTs, mainly because of their faster switching times, and power MOSFETs, mainly because of their lower on-resistance.

DOS is a commonly used concept for a few nanosecond scale pulse generation, because amplitudes can reach up to several kilo-volts. The circuit operates so that the diode with a good repeatability transfers energy saved in the second inductor L_2 , to the load (Fig. 1). In the first, charging period of the generation, the capacitor (C_1) is charged through the resistor (R) by DC voltage supply (V_{IN}). In the beginning of the second discharging period, the switch (S) is turned ON and the energy in the capacitor (C_1) starts circulating in the resonant network (C_1 , C_2 , L_1 , L_2) [27]. If the diode matrix (D) is short-circuited, an

aharmonic oscillation of the current through the inductor L_2 is observed. If the D is not short-circuited, the resonant network firstly pumps current through the diodes. During the forward pumping, charge is accumulated in the diodes PN-junctions [27], which is proportional to the amplitude of the current and the minority carrier lifetime. After completing the half period, the resonant network starts pumping the current through the diodes in the reverse direction. With the charge still present in the PN-junctions, the diodes resume conducting until the accumulated charge is removed. The time which takes to remove the charge is inversely proportional to the amplitude of the current. The ideal DOS abruptly stops conducting and commutates all the L_2 current into the load. The resonant network must be designed in a way that the majority of the energy, firstly stored in C_1 , is stored in L_2 , during the current commutation. This is achieved by doubling the reverse current in comparison to the forward current. During the current commutation the inductor L_2 induces high-voltage pulse on the load in order to maintain the current flow, which is proportional to the $R_L * I_{MAX}$, where R_L is the resistance of the load and I_{MAX} is a maximal reverse current through the diodes. The induced voltage on the load is normally much higher than the charging voltage and the ratio between them is determined by a multiplication factor. The inductors in the resonant network can have ferromagnetic saturable cores which improves the multiplication factor but the generator then operates nonlinearly and only in a small range of output voltages [28]. In contrast, the air-core inductors achieve lower multiplication factor but work linearly from zero voltage to the saturation of semiconductor switches [27].

Most of existing nanosecond pulse generators used for electroporation experiments are based on the pulse forming networks and spark gaps or RF MOSFET switches [22], [29]–[33]. Some DOS pulse generators for electroporation experiments have already been developed and have performed well [23], [22]. Among others, Sanders [27] developed a 5 kV 2.5 ns nanosecond DOS electroporator, Kuthi developed a 1200V 3.5 ns generator [28] and some simulations of the DOS generators have also been done by Kranjc [34].

Measurement of micro- and milli- second electroporation pulses is relatively straightforward as pulse reflections are normally negligible. However, with high-voltage nanosecond pulses, measurement becomes more challenging [23], [35]. Firstly, the electric losses and reflections in the wiring between the generator and the load are no longer negligible, therefore, the probe should be connected to the wiring in electrical proximity to the load. The commercial high-voltage nanosecond probes are costly and useful only in specific setups. Some probes may be incorporated into transmission lines [36] or electrodes [37], other setups may use 50 Ω probes [38] and some must use high-impedance probes [39]. High-voltage nanosecond probes can be made of wide-band resistive voltage divider [39], D-dot sensor [37], 50 Ω probe [38] or capacitive voltage divider [36].

Nanosecond electroporation is being studied for more than a decade, nevertheless the trend still clearly shows increased interest into effects of nanosecond pulses. It is also believed that further investigations of nanosecond electroporation of cells will gain important knowledge necessary for better understanding of

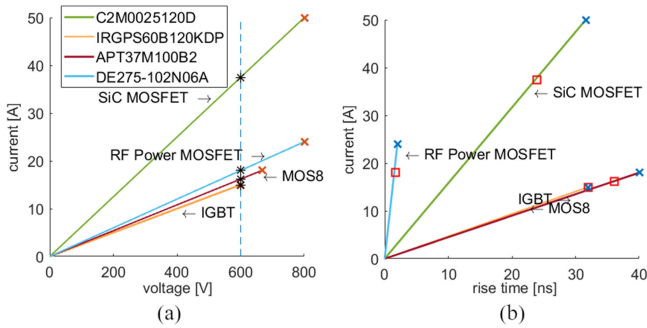


Fig. 2. Comparison of different semiconductor switching technologies which are used for generating nanosecond pulses. Compared are the amplitude (a) and the rise time (b) of the current through the switching element, derived from the data sheets. Currents generated by the switching elements are by linear approximation normalized to the same 600 V supply voltage (red star dots).

dynamics and transport in classical electroporation [40]. Some studies of basic electroporation principles and nanosecond electroporation are still not confirmed or are even contradictory [23]. In case of nanosecond electroporation this can be a result of unique prototype hardware devices, with narrow scope of parameters, incorrect application, or even an incomplete description of used hardware and delivered pulse measurement and characterization [35] or inappropriate measurement equipment or inadequate delivery system. High-voltage nanosecond pulse generators for laboratory use with reproducible pulse delivery of wide range of parameters, as well as accurate high-voltage nanosecond measurement systems are needed.

II. METHODS AND MATERIALS

In nanosecond pulse electroporator design, the main challenge is, to construct a generator that delivers very short and at the same time very high power pulses. The development started with the analysis and comparison between the most commonly used semiconductor switching technologies in pulse generators and silicon carbide (SiC) MOSFET technology (Fig. 2). The comparison was made with switching elements of similar breakdown voltages and sizes, with less than 50 ns rise time, namely DE275-102N06A (RF MOSFET, IXYS, USA), APT37M100B2 (Power MOSFET, Microsemi, USA), IRGFS60B120KDP (IGBT, Infineon, USA) and C2M0025120D (SiC MOSFET, CREE, USA). We have compared the rise time, specified in data sheet and the current amplitude at fixed supply voltage. As different manufacturers test their elements at different supply voltages, we have at first by normalized linear approximation, define test current at rise time data acquisition, which was 600 V (Fig. 2a). SiC technology stand out by the current amplitude. However, with the nanosecond pulses we are also interested in the rate of the current increase. Therefore, we plotted the normalized test current amplitude on the rise time axis (Fig. 2b) on which it can be observed that the current in the SiC MOSFET rises slower than in the RF MOSFET and quicker than in the power MOSFET or IGBT.

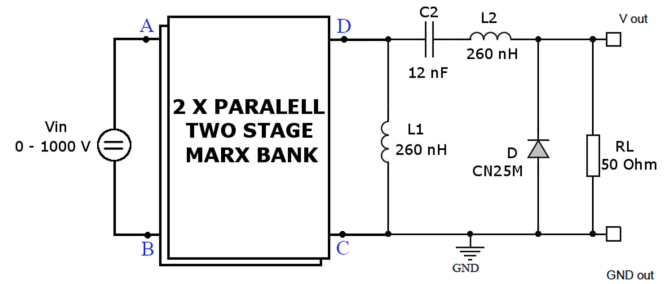


Fig. 3. Basic schematic of DOS generator with two parallel two-stage Marx-banks. Two-stage Marx-bank is used to deliver double voltage to the resonant network in comparison to the breaking voltage of the switch and power supply voltage. Two Marx-banks are used in parallel to deliver higher current to the resonant network. Resonant network (C and L) and DOS (D) are the same as in Sanders linear DOS generator [27].

A. Pulse Generator Design

Further on we focused on DOS generator, which we believe is the most suitable topology for SiC MOSFET based nanosecond pulse generators. With the advantage of using SiC MOSFETs we aimed at developing linear DOS generator that could be used to deliver short nanosecond pulses with wide range of high-voltage amplitudes to the cuvettes. To achieve such high-voltages maximization of I_{MAX} , which is proportional to the $V_{IN} * \sqrt{C_1/L_2}$, is required. However only V_{IN} can be maximized in this equation, as L_2 defines the pulse duration, which should be optimized in accordance with desired biological effect and not for the output voltage. And as C_1 should be calculated so that the reverse recovery time, of the diodes is equal to the $\frac{\pi}{2} \sqrt{C_1 * L_2}$ which consequently enables generation of the output pulse at I_{MAX} . V_{IN} is however, always limited by the breakdown voltage of the switching elements. Therefore, in order to increase the V_{IN} , stacking of the switching elements in series is required. Not to increase the power supply voltage (V_{PS}), a two-stage Marx-bank circuit was used, to stack the switches and two Marx-banks were used in parallel to generate double current in the resonant network (Fig. 3), in comparison to the Sanders linear DOS generator [27]. As we used the same Step Recovery Diodes (SRD) for the DOS (D, CN25M, EIC, Thailand) as Sanders and we did not want to change the pulse duration, the capacitance and inductance of the elements in the resonant network are the same as in the Sanders linear DOS generator. Inductors are air coils, made specially for this application, calibrated with LCR meter (4284A, Agilent), at 1 MHz frequency and 2 V settings.

CN25M diodes have reverse recovery time of 50 ns, maximum repetitive peak reverse voltage 1000 V and maximum average forward current 25 A. Because the maximum reverse voltage of one diode is too low for our application, several diodes must be stacked together in series and as 1000 V divided by 25 A is almost 50 Ω , $n \times n$ matrix of CN25M diodes is the most appropriate for 50 Ω load, where n is the number of diodes in series and in parallel in the matrix. A compact 8 \times 8 diode matrix (Fig. 4) was made by gluing the was made by gluing the diodes together by conductive adhesive (MG chemicals, 8330-19G, 8330S-21G) in order to minimize stray inductance and all parasitic properties of lines connecting the load. The diode

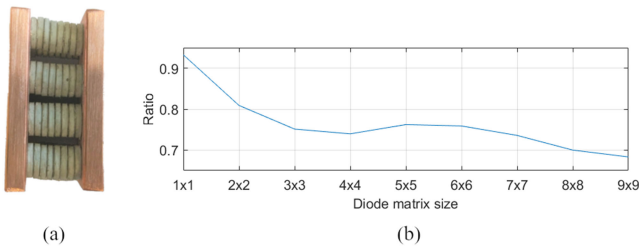


Fig. 4. (a) 8×8 matrix of CN25M diodes glued together with conductive adhesive used in order to minimize stray inductance. (b) Ratio between load current (calculated from the measured voltage) and L_2 current is lower with higher diode matrix size, due to their non-ideal characteristics.

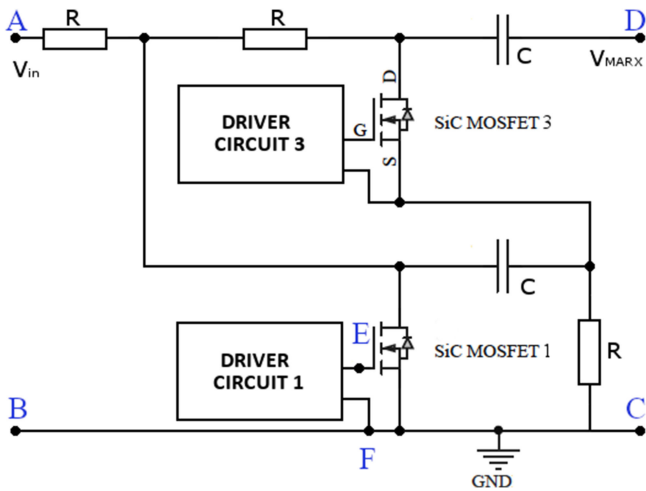


Fig. 5. Schematic of two-stage Marx-bank circuit implemented in the DOS generator. During the charging phase, capacitors (C) are charge parallelly through the resistors (R), and during the discharge phase, SiC MOSFETs connect capacitors in series and discharge them through the resonant network. Two Marx-bank circuits are implemented in parallel to generate high enough current for the resonant network. Each SiC MOSFET has its own driving circuit galvanically separated from each other.

matrix was glued as close as possible to the load and second inductor L_2 . On the (Fig. 4), we can see the ratio between load current (calculated from the measured voltage) and L_2 current. The ratio is lower with higher diode matrix size, due to their non-ideal characteristics. Additionally, all diodes do not stop conducting at exactly the same moment and this may also result in a lower output pulse amplitude as expected. For DOS it would be the best to use custom made diodes.

B. Marx-Bank Circuit

Two-stage Marx-bank circuit (Fig. 5) was developed to enable charging of the resonant network with up to 2000 V. The energy storage capacitors (C) are a part of the Marx-bank circuit and also of the resonant network. During the charging phase the capacitors are parallelly charged through the resistors (R) by the external high-voltage power supply. And during the discharge phase SiC MOSFETs connect capacitors in series and discharge them through the resonant network (Fig. 3). C2M0025120D Silicon Carbide Power MOSFET with N-channel enhancement

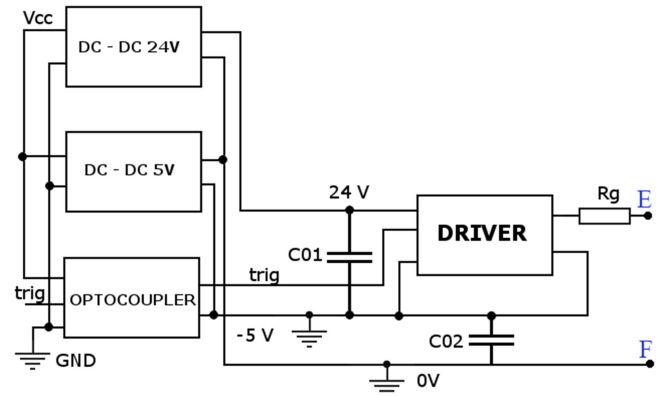


Fig. 6. Block diagram of SiC MOSFET driver circuit. Galvanic separation of the driver is made by isolated DC-DC converters and optocoupler. The driver is supplied by +24 V and -5 V. Power supply capacitors C01 and C02 stabilize the power supply voltage during switching. Gate resistor R_g is used for stable simultaneous switching of all four SiC MOSFETS.

mode (Cree, Inc., USA) were chosen because of their high drain-source breaking voltage, and their high and fast current rise (Fig. 2). It was empirically determined that at least two Marx-bank circuits must be implemented in parallel, to enable generation of high enough currents for the resonant network, before SiC MOSFET reach saturation. Charging resistors have a high value of 2 k Ω to ensure that the capacitors are in the majority discharged through the resonant network. However, due to high resistance of the charging resistors, the energy storage capacitors cannot be instantly recharged and the maximum pulse repetition rate is therefore 3.5 kHz.

C. SiC MOSFET Driving Circuit

When designing a driving circuit for SiC MOSFET (Fig. 6), it is important to consider SiC MOSFETs special characteristics [24]. Due to low transconductance, they must be driven with higher voltage difference than IGBTs or Si MOSFETs. At least 22 V voltage difference is desired for recommended operation, voltage for on stage is 20 V and for off stage from -2 V to -5 V. It is important that the upper limit of 25 V and the lower limit of -10 V are not crossed. Selected SiC MOSFETs start conducting at 2.5 V, but are not totally opened until V_{gs} reaches 16 V. Therefore, high dV/dt of the V_{gs} is needed for fast switching times that means driving circuit should have low impedance. For optimal switching of the SiC MOSFET, stray impedance of the driving circuit must be minimal, therefore, lines connecting the MOSFET driver to power supply capacitors and gate terminal should be as short as possible. Even though the stray impedance is minimized, it can still lead to excessive output oscillations, which can lead to unintentional MOSFET switching that can be suppressed by appropriate gate resistor R_g . The R_g is also important for the simultaneous switching of all four SiC MOSFETs, as asynchronous switching in Marx-bank circuit may overcharge and harm the switches. During the pulse generation, the source (S) electric potential of the first stage switches in the Marx-banks (SiC MOSFET1 and SiC MOSFET2)

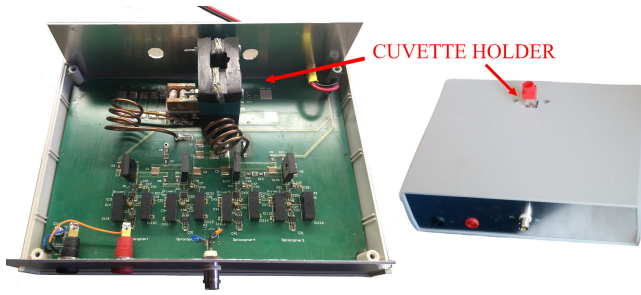


Fig. 7. Final prototype, with open (left) and closed enclosure (right). The cuvette holder is directly connected to the diode matrix in order to minimize parasitic effects.

stay on the same level as the GND (Fig. 5), while the source electric potential of the second stage switches (SiC MOSFET3 and SiC MOSFET4) have to fall to the $-V_{in}$ electric potential of the bottom capacitor (C). The second stage switches must though also charge the stray capacitance, therefore the current through the second stage switches is higher, which slows down their turning on time. To achieve simultaneous switching of the second and first stage switches, the R_g resistance, of the second stage switches, must thus be lower. However, a small difference in rise times should not affect or destroy the MOSFETS, since they operate up to 1200 V. If one of MOSFETS turns on slower, that should not be harmful, until the switching is still fast enough, to prevent the voltage rise of any MOSFET's V_{ds} over 1200 V. In our Marx-bank circuit, we have empirically determined the resistance R_g of the second stage MOSFET's to be 1Ω , and of the first stage to be 2Ω (Fig. 6), to achieve simultaneous switching of all MOSFET's.

Two isolated DC-DC converters (RP-0512D and RP-0505S, RECOM, Germany) are used to power supply the driving circuit and to galvanically separate it from the main power supply lines (Fig. 6). The two DC-DC converters and the source of one SiC MOSFET are connected together to form a 0 V potential for the gate driver. One DC-DC converter then supplies the driver with +24 V and the other with -5 V. Optocoupler (HCPL-0723, Avago USA) is used to galvanically separate the digital trigger signal (trig), and the SiC MOSFETS are driven by an ultrafast MOSFET driver (IXDD609SI, IXYZ, USA). Driver can be supplied with up to 35 V, it can deliver up to 9 A output current and has output resistance of up to 1Ω . The ground of the optocoupler and the driver are connected to the -5 V. The optocoupler is then supplied with 0 V potential for the 5 V supply difference, and the driver with +24 V to have 29 V of operating voltage range. Power supply capacitors C01 and C02 are added to the power supply lines to stabilize the power supply voltage during the switching. As capacitors with different values have different resonant frequencies, C02 is composed of three different capacitors, which result in wider frequency blocking range and better stability of optocoupler's power supply.

D. Fabrication and Assembly

The device (Fig. 7) was implemented on 6U (Eurocard) sized PCB card, it is double sided with $105 \mu\text{m}$ copper layer and solder stop mask. If available, SMD electrical components were

preferably chosen, trigger input connector is a 50Ω BNC and a holder for the electroporation cuvette is made for the output. During the PCB design, special attention was given to make lines in the resonant network and in the output stage spaced enough for the high-voltage, and at the same time as short as possible and wide enough for the high currents. The device is triggered by a function generator (33220A, Agilent Technologies, USA) set to: $V_{PP} = 2.5 \text{ V}$, $f = 1 \text{ kHz}$, pulse length $10 \mu\text{s}$ and offset 1.25 VDC. High-voltage generator (MCP 350-1250, FuG Elektronik GmbH, Germany) and low voltage generator (NG310, UNIWATT, Germany) that supply 5V/3A DC are used for high and low voltage power supply, respectively. Not to damage the DOS in case of too high-impedance of the load, a 100Ω resistor (TFSF100RJE-ND, Ohmite, USA) is added in parallel to the load. If there would not be any load present at pulse generation, DOS would commutate L_2 current to high impedance and L_2 would induce very high voltage, which would damage the DOS and additionally high dv/dt could also damage the optocouplers.

E. Voltage and Current Measurements

For all the voltage and current measurements, an oscilloscope (Wavepro 7300A, LeCroy, USA) was used. Driver circuit was evaluated with differential probes LeCroy ADP305 (1 kV, 100 MHz, LeCroy, USA). The L_2 current in the resonant network was measured by high-frequency current transformer (1 kA, 500 MHz, Bezgoz, France). For the output pulse measurement several different voltage probes were used. The high-voltage output pulse was measured with different commercial probes (HVD3605, PPE20kV, PPE6kV and ADP305, LeCroy, USA), high-voltage commercial attenuators (N-type, J01026A0009, 2.5 kV $20 \text{ dB} \pm 0.8 \text{ dB}$; and BNC, J01006A0837, $20 \text{ dB} \pm 1 \text{ dB}$; both 50Ω , 1GHz, Telegartner, Germany).

III. RESULTS

The nanosecond pulse generator performance was evaluated in three steps. In the first step, driving circuits in the Marx-bank generators were tested for stable simultaneous switching of all four SiC MOSFETS. In the second step, the current in the resonant network was evaluated for the desired waveform and amplitude. And in the third step, the output pulse was measured.

A. SiC MOSFET Driving Circuit

Falling of the voltage V_{DS} on SiC MOSFETS, during the switching, is synchronous. Therefore, no extra voltage is redistributed to the adjacent SiC MOSFETS in the Marx-bank circuits during the switching and the probability for the SiC MOSFET breakdown during the switching is thus minimized. If the power supply voltage, V_{IN} is approximately 700 V or more, V_{DS} after reaching the zero voltage, during the switching, slightly increases because of SiC MOSFET saturation that is due to drain current (I_D) rise. Therefore, the current in the resonant network will not significantly rise with increasing the V_{IN} over 700 V. After the pulse generation, V_{DS} exponentially rises to the supply voltage in approximately $280 \mu\text{s}$ because capacitors C_1 are recharging. Therefore, the maximum pulse repetition rate of the generator that can be reached is 3.5 kHz.

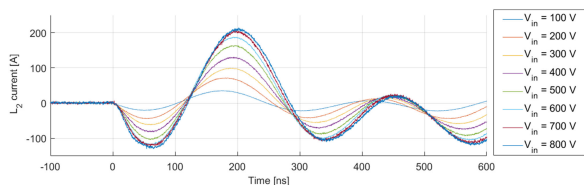


Fig. 8. The waveform of the L_2 current, in the resonant network, is a function of the power supply voltage (V_{IN}). For the analyzes the output of the generator was short circuited. At its maximum, the L_2 current reaches 200 A and the ratio between its first minimum and maximum is 1.7.

B. Resonant Network

The output of the generator was short-circuited and the L_2 current was measured (Fig. 8) to analyze the operation of the resonant network. By increasing the power supply voltage (V_{IN}) the L_2 current linearly increases up to 600 V of V_{IN} and at 700 V it saturates as predicted from the SiC MOSFET switching analyzes. At its maximum the L_2 current reaches 200 A and the ratio between its first current minimum and maximum is 1.7, which meets the expectations and is adequate for nanosecond pulse generation by diode opening switch (DOS) [27].

C. Output Pulse

Measurement of the output pulse of the generator is not straight forward, due to the short duration and at the same time high-voltage. Commercially available high impedance, high voltage probes for measuring voltage amplitudes up to 15 kV have bandwidth in range of 50–70 MHz (-3 dB). Differential 100 MHz probes that can measure up to 6 kV are a better choice for nanosecond pulse measurements, but can still be too slow, due to their rise time, which is around 3 ns. The best choice among commercially available probes for measuring nanosecond pulses are high voltage pulse attenuators that have bandwidths in GHz range and can measure up to 16 kV (Barth electronics, USA), but they are expensive compared to other previously described probes and thus not easily available to all researchers working on nanosecond electroporation field. Therefore, for the evaluation of developed device, a commercially available probes with additional calibration were used. A $50\ \Omega$ commercial attenuators were tested to measure the output pulse. The final attenuator was assembled from two N-type attenuators and one BNC attenuator to achieve $60\ \text{dB} \pm 2.8\ \text{dB}$ attenuation. The factory graded accuracy of the attenuator is still not satisfying, but at least it is possible to calibrate the attenuator satisfactorily, namely, the assembled attenuator measures $31 \pm 2\%$ lower amplitude. The $50\ \Omega$ input of the attenuator of course influences the measurement, but in our case, the load was replaced by the attenuator. With such attenuator, the output pulses of the generator were measured (Fig. 9a). The shape of the pulses is Gaussian, with insignificant reflections. However, because the attenuators graded for 2.5 kV maximum voltage and in our case it broke at 4 kV. Consequently, a commercial high-voltage differential probe (HVD3605, 6 kV, 100 MHz, LeCroy, USA) was used to measure the output voltages over 4 kV. When

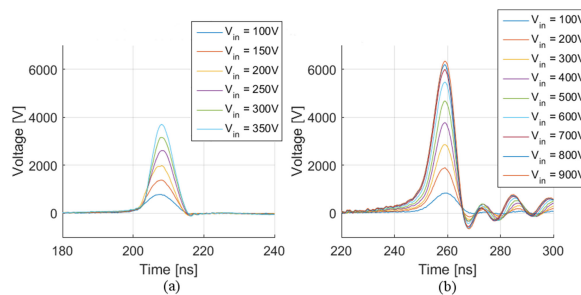


Fig. 9. Output pulse measurements by assembled attenuator (a) and HVD3605 probe (b) as a function of the power supply voltage (V_{IN}). Calculated output pulses taking into account the calibration constants 31% for the assembled attenuator and 5% for the HVD3605 probe.

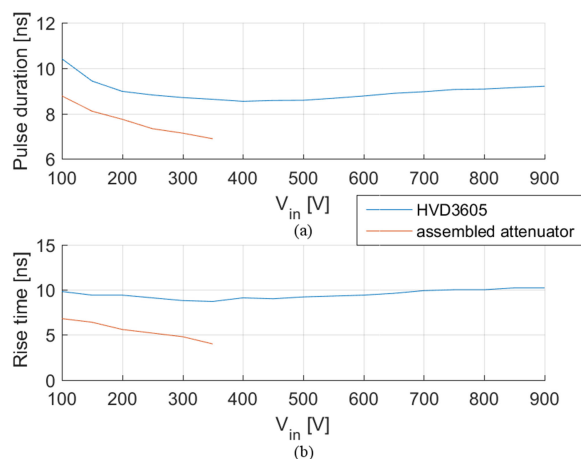


Fig. 10. Duration (a) and rise time (b) of the output pulses in case of assembled attenuator and in case of HVD3605 probe as a function of the power supply voltage (V_{IN}).

the HVD3605 probe is compared with the assembled attenuator a 5% loss in the amplitude is observed and reflections of the pulse arises (Fig. 9b). Measured pulse duration and rise time are shorter if measured with assembled attenuator in comparison to HVD3605 probe (Fig. 10). Pulse duration vary from 7 to 10 ns, while rise time vary from 4 to 10 ns. By increasing the power supply voltage V_{IN} up to 600 V, the amplitude of the output pulse linearly rises (Fig. 11). Over the 600 V of V_{IN} , due to the saturation of the SiC MOSFETs, the rise in the output pulse amplitude gradually declines by increasing the V_{IN} and at 900 V of V_{IN} the rise almost stops. The multiplication factor of the input voltage V_{OUT}/V_{IN} is around 9 in the linear space and in the saturation gradually falls to 7, at 900 V of V_{IN} (Fig. 11). On the figure (Fig. 12) we can see the output pulse amplitude and the FWHM (duration of the pulse) dependency on the load of the developed device. Our generator works as expected, also with cuvette, the amplitude is slightly lower in case of electroporation cuvette than on a $50\ \Omega$ load, while the pulse duration is a bit longer, mainly due to a smaller absolute reactance of the load at generated pulse frequency spectrum [41].

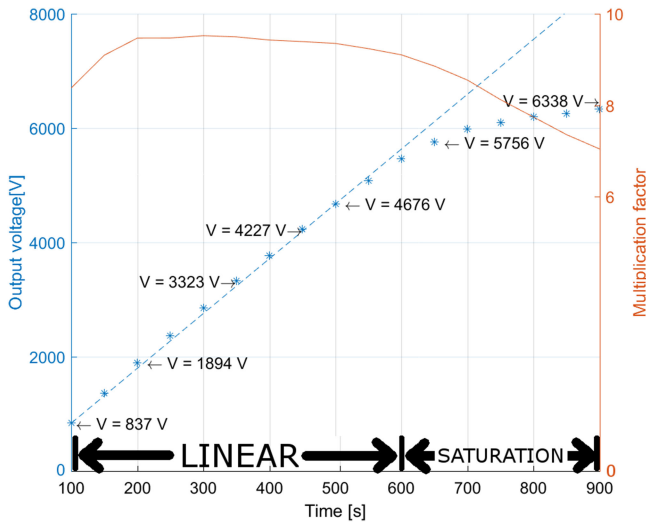


Fig. 11. Output pulse amplitude V_{OUT} as a function of the power supply voltage V_{IN} with linear and saturated space of operation. And the multiplication factor of the input voltage V_{OUT}/V_{IN} .

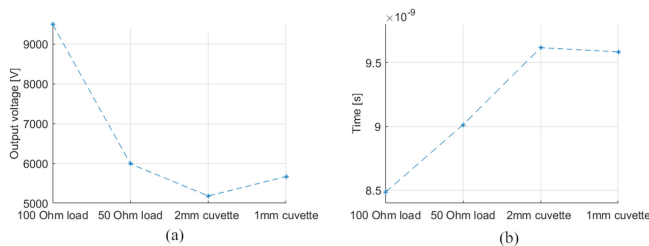


Fig. 12. The comparison of the output pulse amplitude (a) and FWHM (b) generated on different loads. In first two cases we used 100 Ω and 50 Ω load resistor (TFSF100RJE-ND, Ohmite, USA). In second case we added in parallel to 100 Ω load resistor an electroporation cuvette with 1 mm and 2 mm spacing between the electrodes, filled with KPB (Potassium phosphate buffer).

IV. DISCUSSION

The design of the generator is based on a SiC MOSFETs, Marx-bank circuit and DOS. The RF MOSFETs, are still the most appropriate for short nanosecond pulses generated by transmission lines, which require fast rising times (Fig. 2). Whereas the SiC technology is the most suitable technology for longer nanosecond pulses or DOS generators as less elements are needed to generate higher currents. For a SiC MOSFETs a special driver circuit had to be developed that delivers the negative voltage on the gate during the off stage. For the correct operation of the Marx-bank circuit, the power supply and the control signal of the driver have to be properly galvanically isolated and the gate resistors have to be optimized for simultaneous switching of all four SiC MOSFETs. Otherwise, electrical elements could be damaged during the switching, especially the SiC MOSFETs and the optocouplers. The current in the resonant network could be increased by embedding one or two more Marx-bank circuits in parallel. Nevertheless, 200 A appeared to be enough for our aim [42]. However, the resonant network and DOS configuration that were taken from the previous publication [27] did not work as expected. The rise time of the output pulse was much longer

than expected, consequently, also the amplitude of the output pulse was not as high as expected. The causes for this under performance could be a mismatched frequency of the resonant network with reverse recovery time of the DOS, or the stray impedance on the generator's output. Even though, the amplitude of the output pulse was not as high as expected, the multiplication factor V_{OUT}/V_{IN} is approximately 9, which is still an improvement compared to the previously published linear DOS generator [27]. The improvement was achieved primarily through the use of SiC MOSFETs which enable more current and Marx-bank circuit which in the same time delivers double voltage to the LC oscillator. If the DOS would work as fast as in the previous publication of the linear DOS generator, it is expected that the multiplication factor would be 14. However, the biggest challenge was to adequately evaluate the output pulse. Researchers in the field of nanosecond electroporation use various methods to measure the high-voltage nanosecond pulses [36]–[39]. Due to conditional usability and high costs, of commercial probes, the researchers often develop their own high-voltage nanosecond probes. Also more costly commercial high-voltage differential probes, for example HVD3605 probe (LeCroy, USA), can be used for high-voltage nanosecond pulse measurement. These probes are very accurate in their wide bandwidth, however, at the limit of the bandwidth, due to not the most suitable connection terminals, the pulse reflection occurs and the probe loses accuracy, but not more than -3 dB. For this reason, we evaluated measuring error that occurs during the output pulse measurement. The commercial calibrated RF attenuators and the HVD3605 differential voltage probe were evaluated. Because HVD3605 is not very accurate at high-frequency signals, we would suggest that a high voltage -20 dB attenuator is made, or bought and then calibrated. And also that the commercial wide band 50 Ω attenuators are used to attenuate the signal to the oscilloscope's voltage level. Thus, each attenuator could be accurately calibrated and the measurement of the high-voltage nanosecond pulse would be more accurate. For the high-voltage attenuator, we suggest using capacitive voltage divider if we do not want to influence the measured signal, otherwise the 50 Ω attenuator should be the most accurate and appropriate.

V. CONCLUSION

A nanosecond pulse generator was developed for “in vitro” electroporation experiments using standard electroporation cuvettes. The generator can deliver from 500 V to more than 6 kV, approximately 8 ns pulses to a 50 Ω load. Two in parallel two-stage Marx-bank circuits can generate up to 200 A current in the resonant circuit. As the SiC MOSFETs already go into saturation at 600 V (Fig. 11). However, the biggest challenge in this study was to accurately measure the high-voltage short nanosecond pulses. We have already emphasized [23] that accurate measurement of the delivered nanosecond pulses is crucial for the unbiased nanosecond electroporation experiments. But it should be also emphasized that the bandwidth of the probes ends at -3 dB which means that the probe at the end of its bandwidth has a -29% error. A -29% error may be acceptable for electronics, however, a 29% different amplitude may have a significantly different biological effect [43], [44].

Because permeabilization and cell survival are sigmoid functions of voltage, more than 10% difference in voltage may result in a significantly different biological effect. For example, if we focus on permeabilization curve, a $\pm 29\%$ deviation from the real voltage amplitude result in totally different outcome. In one case the majority of cells can be intact (i.e., not permeabilized) while in other case, the majority of the cells can be permeabilized [43], [44]. Whenever we are using measuring probes, we have to be aware of the measuring error. Commercially available probes have the measuring error specified in a data sheet, but it is still sometimes overlooked, while prototype probes have to be correctly calibrated and measuring error evaluated.

ACKNOWLEDGMENT

The authors would like to thank Philippe Lévêque and Delia Arnaud-Cormos, from XLIM Research Institute at University of Limoges, France for the help at work that apply to nanosecond pulse measurement techniques.

REFERENCES

- J. C. Weaver, "Electroporation of cells and tissues," *IEEE Trans. Plasma Sci.*, vol. 28, no. 1, pp. 24–33, Feb. 2000.
- C. Chen *et al.*, "Membrane electroporation theories: A review," *Med. Biol. Eng. Comput.*, vol. 44, no. 1–2, pp. 5–14, 2006.
- T. Kotnik *et al.*, "Membrane electroporation and electropermeabilization: Mechanisms and models," *Annu. Rev. Biophys.*, vol. 48, pp. 63–91, 2019.
- M. L. Yarmush *et al.*, "Electroporation-based technologies for medicine: Principles, applications, and challenges," *Annu. Rev. Biomed. Eng.*, vol. 16, pp. 295–320, 2014.
- S. Haberl *et al.*, "Cell membrane electroporation—Part 2: The applications," *IEEE Elect. Insul. Mag.*, vol. 29, no. 1, pp. 29–37, Jan./Feb. 2013.
- B. Mali *et al.*, "Antitumor effectiveness of electrochemotherapy: A systematic review and meta-analysis," *Eur. J. Surgical Oncol.*, vol. 39, no. 1, pp. 4–16, 2013.
- E. Pirc *et al.*, "Study design of a medical device pre-market assessment: A case study on electrochemotherapy," *Slovenian Med. J.*, vol. 87, no. 1–2, pp. 22–40, 2018.
- T. Stepisnik *et al.*, "Electrochemotherapy – an effective method for the treatment of tumors with a combination of chemotherapeutic agent and electric field," *Slovenian Med. J.*, vol. 85, no. 1, pp. 41–55, 2016.
- H. J. Scheffer *et al.*, "Irreversible electroporation for nonthermal tumor ablation in the clinical setting: A systematic review of safety and efficacy," *J. Vascular Interventional Radiol.*, vol. 25, no. 7, pp. 997–1011, 2014.
- B. Rubinsky, "Irreversible electroporation in medicine," *Technol. Cancer Res. Treatment*, vol. 6, no. 4, pp. 255–260, 2007.
- M. Golzio *et al.*, "Direct visualization at the single-cell level of electrically mediated gene delivery," *Proc. Nat. Acad. Sci.*, vol. 99, no. 3, pp. 1292–1297, 2002.
- M. Coustets *et al.*, "Flow process for electroextraction of total proteins from microalgae," *J. Membrane Biol.*, vol. 246, no. 10, pp. 751–760, 2013.
- I. P. Sugar *et al.*, "Model of cell electrofusion: Membrane electroporation, pore coalescence and percolation," *Biophysical Chem.*, vol. 26, no. 2, pp. 321–335, 1987.
- O. N. Pakhomova *et al.*, "Facilitation of electroporative drug uptake and cell killing by electrosensitization," *J. Cellular Mol. Med.*, vol. 17, no. 1, pp. 154–159, 2013.
- C. Luft and R. Ketteler, "Electroporation knows no boundaries: The use of electrostimulation for siRNA delivery in cells and tissues," *J. Biomolecular Screening*, vol. 20, no. 8, pp. 932–942, 2015.
- A. Golberg *et al.*, "Energy-efficient biomass processing with pulsed electric fields for bioeconomy and sustainable development," *Biotechnol. Biofuels*, vol. 9, no. 1, pp. 1–22, 2016.
- G. Pucihar *et al.*, "Equivalent pulse parameters for electroporation," *IEEE Trans. Biomed. Eng.*, vol. 58, no. 11, pp. 3279–3288, Nov. 2011.
- T. Kotnik and D. Miklavčič, "Theoretical evaluation of voltage induction on internal membranes of biological cells exposed to electric fields," *Biophys. J.*, vol. 90, no. 2, pp. 480–491, 2006.
- M. Reberšek *et al.*, "Cell membrane electroporation—Part 3: The equipment," *IEEE Elect. Insul. Mag.*, vol. 30, no. 3, pp. 8–18, May–Jun. 2014.
- E. Pirc *et al.*, "Dosimetry in electroporation-based technologies and treatments," in *Dosimetry in Bioelectromagnetics*, M. S. Markov, Ed., Boca Raton, FL, USA: CRC Press, 2017, pp. 233–268.
- L. Chopinet *et al.*, "Nanosecond electric pulse effect on gene expression," *J. Membrane Biol.*, vol. 246, no. 11, pp. 851–859, 2013.
- R. Sundararajan, "Nanosecond electroporation: Another look," *Mol. Biotechnol.*, vol. 41, no. 1, pp. 69–82, 2009.
- T. Batista Napotnik *et al.*, "Effects of high voltage nanosecond electric pulses on eukaryotic cells (in vitro): A systematic review," *Bioelectrochemistry*, vol. 110, pp. 1–12, 2016.
- L. D. Stevanovic *et al.*, "Recent advances in silicon carbide MOSFET power devices," in *Proc. 25th Annu. IEEE Appl. Power Electron. Conf. Expo.*, 2003, pp. 401–407.
- V. Novickij *et al.*, "High-frequency submicrosecond electroporator," *Biotechnol. Biotechnol. Equip.*, vol. 30, no. 3, pp. 607–613, 2016.
- D. M. Brown *et al.*, "Silicon carbide MOSFET technology," *Solid-State Electron.*, vol. 39, no. 11, pp. 1531–1542, 1996.
- J. M. Sanders *et al.*, "A linear, single-stage, nanosecond pulse generator for delivering intense electric fields to biological loads," *IEEE Trans. Dielectr. Elect. Insul.*, vol. 16, no. 4, pp. 1048–1054, Aug. 2009.
- A. Kuthi *et al.*, "Nanosecond pulse generator using fast recovery diodes for cell electromanipulation," *IEEE Trans. Plasma Sci.*, vol. 33, no. 4, pp. 1192–1197, Aug. 2005.
- J. F. Kolb *et al.*, "Nanosecond pulsed electric field generators for the study of subcellular effects," *Bioelectromagnetics*, vol. 27, no. 3, pp. 172–187, 2006.
- S. R. Rajulapati *et al.*, "Nanosecond biphasic pulse generators for biomedical applications," in *Proc. Abstr. IEEE Int. Conf. Plasma Sci.*, 2013, pp. 1–4.
- M. Reberšek *et al.*, "Blumlein configuration for high-repetition-rate pulse generation of variable duration and polarity using synchronized switch control," *IEEE Trans. Biomed. Eng.*, vol. 56, no. 11, pp. 2642–2648, Nov. 2009.
- T. Tang *et al.*, "Diode opening switch based nanosecond high voltage pulse generators for biological and medical applications," *IEEE Trans. Dielectr. Elect. Insul.*, vol. 14, no. 4, pp. 878–883, Aug. 2007.
- J. M. Sanders *et al.*, "Optimization and implementation of a solid state high voltage pulse generator that produces fast rising nanosecond pulses," *IEEE Trans. Dielectr. Elect. Insul.*, vol. 18, no. 4, pp. 1228–1235, Aug. 2011.
- M. Kranjc *et al.*, "Numerical simulations aided development of nanosecond pulse electroporators," in *Proc. 6th Eur. Conf. Antennas Propag.*, 2012, pp. 344–347.
- M. Reberšek, "Beyond electroporation pulse parameters: From application to evaluation," in *Handbook of Electroporation*, D. Miklavčič, Ed., Berlin, Germany: Springer, 2017.
- T. J. Camp *et al.*, "Bioelectric studies with subnanosecond pulsed electric fields," in *Proc. IEEE Pulsed Power Conf.*, 2009, pp. 876–879.
- A. Silve *et al.*, "Implementation of a broad band, high level electric field sensor in biological exposure device," in *Proc. IEEE Int. Power Modulator High Voltage Conf.*, 2010, pp. 711–714.
- P. Leveque and D. Arnaud-Cormos, "Measurement and characterization of exposure systems for high-frequency, ultrashort pulses," in *Handbook of Electroporation*, D. Miklavčič, Ed., Berlin, Germany: Springer, 2017.
- J. M. Sanders *et al.*, "Broadband power measurement of high-voltage, nanosecond electric pulses for biomedical applications," in *Proc. IEEE Int. Power Modulators High Voltage Conf.*, 2008, pp. 350–353.
- A. T. Esser *et al.*, "Mechanisms for the intracellular manipulation of organelles by conventional electroporation," *Biophysical J.*, vol. 98, no. 11, pp. 2506–2514, 2010.
- M. Kenaan *et al.*, "Characterization of a 50- Ω exposure setup for high-voltage nanosecond pulsed electric field bioexperiments," *IEEE Trans. Biomed. Eng.*, vol. 58, no. 1, pp. 207–214, Jan. 2011.
- E. B. Garon *et al.*, "In vitro and in vivo evaluation and a case report of intense nanosecond pulsed electric field as a local therapy for human malignancies," *Int. J. Cancer*, vol. 121, no. 3, pp. 675–682, 2007.
- I. Semenov *et al.*, "Primary pathways of intracellular Ca²⁺ mobilization by nanosecond pulsed electric field," *Biochimica et Biophysica Acta (BBA) – Biomembranes*, vol. 1828, no. 3, pp. 981–989, 2013.
- W. E. Ford *et al.*, "Nanosecond pulsed electric fields stimulate apoptosis without release of pro-apoptotic factors from mitochondria in B16f10 Melanoma," *Arch. Biochemistry Biophys.*, vol. 497, no. 1, pp. 82–89, 2010.